2.5D EM modeling in TIV conductive media

Torgeir Wiik*, Bjørn Ursin* and Ketil Hokstad*,†

**Norwegian University of Science and Technology,*

Department for Petroleum Engineering and Applied Geophysics,

S.P. Andersens vei 15A,

NO-7491 Trondheim, Norway

torgeir.wiik@ntnu.no

bjorn.ursin@ntnu.no

†*Statoil Research Centre,*

Arkitekt Ebbells veg 10,

NO-7053 Ranheim, Norway

kehok@statoilhydro.com

(October 17, 2010)

1

Running head: **2.5D TIV EM Modeling**

ABSTRACT

We present an integral equation framework for 2.5D frequency domain EM modeling in conductive media, i.e. in media which are assumed invariant in one direction. Further, we consider media which are transversely isotropic in the vertical direction

(TIV), thus allowing the horizontal and vertical conductivities to differ. The geometrical information concerning model invariance is utilized in the 3D equations by applying a Fourier transform in the invariant direction, which reduces the problem from solving a 3D equation to solving a limited set of 2D equations. This approach has applications in mCSEM modeling of single line data when there is little medium variation cross line. The integral equation framework allows for discretization of only a very limited area of the model given a proper background model, thus leading to a small system of equations to be solved. The numerical examples show that the 2.5D integral equation framework is able to model mCSEM experiments with TIV anisotropy, and that anisotropy has a significant effect on mCSEM data. We further demonstrate that the presence of TIV anisotropy in the overburden may screen a resistor and make it harder to detect. TIV anisotropy should thus be taken into account when modeling mCSEM data to possibly avoid wrongful conclusions.

INTRODUCTION

Electromagnetics is a classical topic in physics and is well explored, but the use of electromagnetic signals for hydrocarbon prospecting is a relatively new achievement (Eidesmo et al., 2002). Due to the fact that a hydrocarbon reservoir typically possesses a low electric conductivity compared to its surroundings in the subsurface the reservoir will act as a wave guide for the low-frequency electromagnetic signal ($0.1 - 10$Hz) used in marine Controlled Source ElectroMagnetic (mCSEM) surveys. The signal then leaks towards the surface from the resistive waveguide and is recorded at the seabed (Løseth, 2007). Due to the low conductivity in the reservoir, the signal traveling within this resistive area is not as attenuated as that propagating outside. Thus, at long source/receiver offsets this scattered signal will have a significant impact on the recorded signal (Eidesmo et al., 2002; Kong et al., 2002). Further, these recorded data also contain effects due to anisotropy in the subsurface (Løseth and Ursin, 2007). Hence, modeling tools to describe this process is crucial to understand the propagation of electromagnetic fields in a given model and for interpretation of mCSEM data.

We will describe how to use integral equation (IE) modeling to compute the frequency domain response from a known model which is invariant in the direction orthogonal to a single line of sources/receivers (cross line), when it is illuminated by a known source. As many mCSEM surveys are still collected along lines this could be useful in many situations. We first briefly present the general IE framework for 3D anomalies, explored earlier by e.g. Hohmann (1975, 1983); Zhdanov (2002); Abubakar

and van den Berg (2004), and then demonstrate how to simplify this in the case of media which are invariant in one direction, so called 2.5D. We formulate the method for conductive media which are transversely isotropic in the vertical direction (TIV) and test it on mCSEM scale models. By TIV anisotropy we mean that the currents induced by the source signal prefer either the horizontal or vertical direction over the other, possibly due to some specific grain orientation (Negi and Saraf, 1989).

Even though the geometry in this problem is then 2D we may not use 2D equations, as this would not yield 3D field characteristics. We utilize this information in the 3D equations by applying a Fourier transform in the invariant direction. This reduces the problem numerically to solving a limited set of 2D problems, in stead of a 3D problem. 2.5D IE modeling of mCSEM data in TIV media has to the authors' knowledge not been published earlier. The IE framework is an effective method in settings where suitable background Green's functions can be simulated quickly, as only a smaller domain inside the background needs to be discretized. Although resulting in a full system matrix, it is often significantly smaller than those arising from finite difference or finite element methods.

The 2.5D approach to geophysical EM modeling is not a new idea. A brief mention of the IE framework is given in (Hohmann, 1987), together with a review of 2D and 3D modeling. Tehrani and Slob (2008) compared 2.5D and 3D IE modeling in isotropic models, and Abubakar et al. (2006) considered 2.5D modeling using isotropic models in cross well configurations. We note that the 2.5D approach has also been explored previously using other methods, such as finite element methods, see e.g. Unsworth

et al. (1993); Mitsuhata (2000); Li and Key (2007); Kong et al. (2008), and finite differences (Stoyer and Greenfield, 1976; Abubakar et al., 2008). Hohmann (1971) considered scattering from two-dimensional scattering objects in the field from a line source current using integral equations.

Upon formulating the 2.5D TIV problem we present three numerical examples. We show that this 2.5D approach is feasible for mCSEM scale problems, and as the problem is reduced to solving a limited number of 2D problems it should prove computationally less intensive than a full 3D approach. Thus, when the setting allows it, it could be favorable with 2.5D IE mCSEM modeling compared to full 3D modeling. Further, the numerical examples show that TIV anisotropy has a significant effect on the recorded response which should be taken into account. For instance, we show that TIV anisotropy in the overburden may screen an anomaly below and make it harder to detect.

THEORY

Governing equations

It is well known that in the frequency domain the electric field vector $\mathbf{e} = [e_x, e_y, e_z]$ and magnetic field strength vector $\mathbf{h} = [h_x, h_y, h_z]$, in a domain without magnetic anomalies, satisfy (Stratton, 1941)

$$\nabla \times \mathbf{e} = \mathrm{i}\omega\mu_0\mathbf{h}, \tag{1}$$

$$\nabla \times \mathbf{h} = \tilde{\boldsymbol{\sigma}}_0\mathbf{e} + \mathbf{j}^S, \tag{2}$$

where $\mathrm{i} = \sqrt{-1}$, ω is the angular frequency, $\mu_0 = 4\pi \cdot 10^{-7}\mathrm{N/A}^2$ is the vacuum magnetic permeability, $\mathbf{j}^S$ is the electric source current vector, $\tilde{\boldsymbol{\sigma}}_0 = \boldsymbol{\sigma}_0 - \mathrm{i}\omega\epsilon_0\mathbf{I}$ and $\mathbf{I}$ is the identity tensor. Here $\boldsymbol{\sigma}_0$ and ϵ_0 denote the electric conductivity and permittivity of a given background model, respectively, and we have accepted Ohm's law (Stratton, 1941)

$$\mathbf{j} = \boldsymbol{\sigma}\mathbf{e}. \tag{3}$$

We further assume a TIV medium, thus considering the conductivity to be a dyad of the form (Løseth and Ursin, 2007)

$$\boldsymbol{\sigma} = \begin{pmatrix} \sigma_h & 0 & 0 \\ 0 & \sigma_h & 0 \\ 0 & 0 & \sigma_v \end{pmatrix}. \tag{4}$$

In the mCSEM setting it is customary to neglect the displacement currents in the subsurface, due to the conductive media and the low frequencies (Nabighian, 1987), using $\tilde{\boldsymbol{\sigma}}_0 = \boldsymbol{\sigma}_0$.

The electric and magnetic Green's tensors, $\mathbf{G}^E$ and $\mathbf{G}^H$, are defined as the impulse response of the background medium due to an electric point source (Green, 1828),

and are thus given by the equations

$$\nabla \times \mathbf{G}^E(\mathbf{x}, \mathbf{x}_0) = \mathrm{i}\omega\mu_0 \mathbf{G}^H(\mathbf{x}, \mathbf{x}_0), \tag{5}$$

$$\nabla \times \mathbf{G}^H(\mathbf{x}, \mathbf{x}_0) = \tilde{\boldsymbol{\sigma}}_0 \mathbf{G}^E(\mathbf{x}, \mathbf{x}_0) + \mathbf{I}\delta(\mathbf{x} - \mathbf{x}_0), \tag{6}$$

where $\mathbf{x} = (x, y, z)$ is a point in space, $\mathbf{x}_0$ is the source position and δ is Dirac's delta function. The divergence equations in Maxwell's equations are also imposed.

The solution to equations 1 and 2 in the given background medium is then given component wise by (Hohmann, 1983)

$$e_i = \int_{\mathbb{R}^3} G_{ij}^E(\mathbf{x}, \mathbf{x}') j_j^S(\mathbf{x}') \, \mathrm{d}\mathbf{x}', \tag{7}$$

$$h_i = \int_{\mathbb{R}^3} G_{ij}^H(\mathbf{x}, \mathbf{x}') j_j^S(\mathbf{x}') \, \mathrm{d}\mathbf{x}', \tag{8}$$

when written according to Einstein's rule of summation, i.e. summing over all repeated indices. Here $i, j \in \{x, y, z\}$ and G_{ij}^E / G_{ij}^H denotes component (i, j) of the corresponding dyad.

Consider now a background model $\mathcal{B}$ in which there is an anomaly in electric conductivity, $\boldsymbol{\sigma}$, compared to the background. Assume further that this anomaly is enclosed in a finite domain $\mathcal{D}$ in which there are no electrical sources present. See Figure 1 for a schematic figure of this. We denote the conductivity inside this domain as $\boldsymbol{\sigma} = \boldsymbol{\sigma}(\mathbf{x})$. According to equations 1 and 2 the electric and magnetic fields inside $\mathcal{D}$ satisfy

$$\nabla \times \mathbf{e} = \mathrm{i}\omega\mu_0\mathbf{h}, \tag{9}$$

$$\nabla \times \mathbf{h} = \tilde{\sigma}_0\mathbf{e} + (\boldsymbol{\sigma} - \boldsymbol{\sigma}_0)\,\mathbf{e}. \tag{10}$$

This implies that $\mathbf{j}^S = \sigma_{0,v}\boldsymbol{\chi}\mathbf{e}$ inside $\mathcal{D}$, where

$$\boldsymbol{\chi} = \begin{pmatrix} \chi_h & 0 & 0 \\ 0 & \chi_h & 0 \\ 0 & 0 & \chi_v \end{pmatrix} = \begin{pmatrix} \frac{\sigma_h}{\sigma_{0,v}} - \frac{\sigma_{0,h}}{\sigma_{0,v}} & 0 & 0 \\ 0 & \frac{\sigma_h}{\sigma_{0,v}} - \frac{\sigma_{0,h}}{\sigma_{0,v}} & 0 \\ 0 & 0 & \frac{\sigma_v}{\sigma_{0,v}} - 1 \end{pmatrix}, \tag{11}$$

is a dimensionless contrast. If $\mathcal{D}$ is illuminated by a source from the outside, we may now according to equation 7 write the total electric field at a point inside $\mathcal{D}$ as (Zhdanov, 2002)

$$e_i = e_i^{\mathrm{inc}} + \int_{\mathcal{D}} G_{ij}^E \sigma_{0,v}\chi_{jj}e_j \mathrm{d}\mathbf{x}', \tag{12}$$

where $\mathbf{e}^{\mathrm{inc}}$ is the incident electric field from the electric source and the integral term represents the scattered field due to the conductivity difference. Equation 12 is equivalent with the Lippmann-Schwinger equation for the scalar Helmholtz equation (Colton and Kress, 1992). For simplicity we have omitted to denote the arguments. Assuming that we are able to solve equation 12 for the electric field inside $\mathcal{D}$ we may now express the scattered fields at receiver points outside $\mathcal{D}$ as

$$f_i^E = \int_{\mathcal{D}} G_{ij}^E \sigma_{0,v} \chi_{jj} e_j \mathrm{d}\mathbf{x}', \tag{13}$$

$$f_i^H = \int_{\mathcal{D}} G_{ij}^H \sigma_{0,v} \chi_{jj} e_j \mathrm{d}\mathbf{x}'. \tag{14}$$

After determining the scattered fields, the total fields are determined by superimposing them with the incident fields given by equations 7 and 8.

2.5D scattering

We now assume a 3D setting with medium invariance in the cross line direction (y) to the sailing direction (x), and thus let a single source/receiver line be placed at $y = 0$ and along the x-direction. The source polarization is also assumed to be in the x-direction. The geometry is then invariant in the y-direction, and it is really 2D.

The goal of the 2.5D approach is to reduce the computational complexity of the modeling problem under the condition of cross line invariance. A true 3D source is required to obtain correct 3D field characteristics, as opposed to solving the corresponding 2D problem. Thus, we seek to utilize the information regarding model invariance to reduce the complexity, while still obtaining true field characteristics.

Under these assumptions we have

$$\boldsymbol{\chi} = \boldsymbol{\chi}(\mathbf{x}) = \boldsymbol{\chi}(\mathbf{x}_T), \tag{15}$$

where $\mathbf{x}_T = (x, z)$, and we define the spatial Fourier transform

$$\hat{u}\left(k_y\right) = \int_{\mathbb{R}} e^{\mathrm{i}k_y y} u\left(y\right) \mathrm{d}y, \tag{16}$$

and the appropriate normalized inverse transform. We proceed by applying this transform to equations 12, 13 and 14. Due to the medium invariance assumption and the convolutional structure, the y-integration reduces to a spectral multiplication and we obtain (Hohmann, 1987)

$$\begin{aligned}
\hat{e}_i &= \hat{e}_i^{\mathrm{inc}} + \int_{\mathbf{x}_T \in \mathcal{D}} \hat{G}_{ij}^E \sigma_{0,v} \chi_{jj} \hat{e}_j \mathrm{d}\mathbf{x}'_T, & (17)\\
\hat{f}_i^E &= \int_{\mathbf{x}_T \in \mathcal{D}} \hat{G}_{ij}^E \sigma_{0,v} \chi_{jj} \hat{e}_j \mathrm{d}\mathbf{x}'_T, & (18)\\
\hat{f}_i^H &= \int_{\mathbf{x}_T \in \mathcal{D}} \hat{G}_{ij}^H \sigma_{0,v} \chi_{jj} \hat{e}_j \mathrm{d}\mathbf{x}'_T. & (19)
\end{aligned}$$

The equations presented so far in this section constitute the 2.5D framework for calculating the electromagnetic field response at a receiver location in the wavenumber domain. Our ultimate goal is to calculate the electromagnetic response in the space domain, so the strategy is to solve the 2.5D equations 17-19 for a proper set of wavenumbers k_y, and then perform an inverse Fourier transform numerically. We note that the problem is then reduced from a full 3D problem to solving a set of 2D problems for different k_y, as the integrals are now two-dimensional.

To solve equation 17 we use the conjugate gradient method described by van den Berg (1984), and the inverse Fourier transform is performed using cubic spline interpolation between the selected wavenumbers (Unsworth et al., 1993; Mitsuhata, 2000). To ensure that a sufficient selection of wavenumbers is chosen we combine the

strategies mentioned in Mitsuhata (2000); Abubakar et al. (2006); Kong et al. (2008), which give an upper bound and a guideline for the selection.

NUMERICAL EXAMPLES

1D benchmark

To validate our implementation we test our code against a TIV 1D code based on the theory described by e.g. Ursin (1983); Løseth and Ursin (2007). We choose a layered background which consists of a 500m water column with conductivity 3.2S/m below a free surface, and a homogeneous subsurface with conductivity 1S/m. At $1500-1600$m below the free surface we have placed an anisotropic resistor with $\sigma_h = 0.1$S/m and $\frac{\sigma_h}{\sigma_v} = 4$. The model used is shown in Figure 2, and the domain $\mathcal{D}$ was chosen at $-10000\text{m} \leq x \leq 10000\text{m}$, $1500\text{m} \leq z \leq 1600\text{m}$, which gives $400 \times 5 = 2000$ grid cells to determine the electric field components in. $\mathcal{D}$ was discretized using $\Delta x = 50$m and $\Delta z = 20$m. The source in Figure 2, placed at $x = 0$m, $z = 450$m, is chosen as an electric point source with unit dipole moment, operating frequency of 0.25Hz, and is polarized in the x-direction. The receivers are placed at $z = 500$m, and $-8000\text{m} \leq x \leq 8000\text{m}$ with an uniform spacing of 500m.

We choose the spectral values k_y such that the incident field at the receivers has an upper bound of 5% relative error when comparing the Fourier transformed 2.5D fields with the 3D fields, and end up choosing in total 25 spectral values distributed in the range 0m^{-1} to 0.05m^{-1}. This number of wavenumbers is in accordance with

the number of wavenumbers used by e.g. Mitsuhata (2000) and Kong et al. (2008). The results are shown in Figures 3 - 6, which display the 2.5D results for the inline and vertical **e**-field in the same axis as the 1D results, and normalized amplitudes and phase differences, respectively.

We see from the figures that both amplitude and phase comply with the 1D results, and the error is stable at a level corresponding to the criterion for choosing the wavenumbers. We notice that the phase differences in the inline and vertical components are very similar, although not equal. In Figures 3 and 5 we also clearly notice the difference between the results with anisotropy present and when the resistor is isotropic with the horizontal conductivity. This is because the response is governed by the vertical conductivity (Løseth, 2007).

Comparison with previous results

We have here repeated the exercise performed by Kong et al. (2008), simulating the response from the model in their Figure 8. We present our equivalents of Figures 9 and 10 in the mentioned paper. The model is a stratified earth with horizontal resistivities ranging from 1Ohm-m to 3Ohm-m, and anisotropy coefficients $\frac{\sigma_h}{\sigma_v}$ from 1 to 3. The water depth is 300m. Between 0m $\leq x \leq$ 10000m, 1430m $\leq z \leq$ 1450m a 50Ohm-m resistor has been inserted, while elsewhise this layer has a 1Ohm-m horizontal resistivity and anisotropy coefficient $\frac{\sigma_h}{\sigma_v} = 2$. We choose our background model as their stratified model where the 20m thick layer is removed and replaced by the properties of the layer beneath. The domain $\mathcal{D}$ is chosen as $-12000\text{m} \leq x \leq 12000\text{m}$,

1430m $\leq z \leq$ 1450m, where the coordinate system is shifted compared to that in Kong et al. (2008) such that the source is placed at $x = 0$m. Inside $\mathcal{D}$ we specify the contrast such that it is in compliance with the model from Kong et al. (2008). The discretization is $\Delta x = 50$m, $\Delta z = 5$m, which amounts to 1920 grid cells only, compared to the approximately 5000 nodes indicated in Kong et al. (2008).

The equivalents of Figures 9 and 10 from Kong et al. (2008) are shown in Figures 7 and 8. In Figure 7 the 1D results refer to a model where the 20m thick layer has 1Ohm-m horizontal resistivity and $\frac{\sigma_h}{\sigma_v} = 2$, while for Figure 8 the layer has 50Ohm-m resistivity. We observe the same properties as Kong et al. (2008) with a match for negative offsets when no target is present in the 1D model, while when the target is present in the 1D model the results matches approximately at positive offsets. The match is better for the prior situation.

Anisotropic overburden

To investigate the effect of an anisotropic overburden on the mCSEM response from a resistor we consider the model shown in Figure 9. The domain $\mathcal{D}$ was chosen as -5000m $\leq x \leq$ 15000m, 900m $\leq z \leq$ 1550m with mesh-size $\Delta x = 50$m, $\Delta z = 10$m, such that we model the anisotropy with the 2.5D code. The source is again an electric dipole with unit dipole moment, operating frequency of 0.25Hz, polarized inline, and positioned at $x = 0$m, $z = 450$m, while the receivers are equidistantly placed on the seabed with a spacing of 500m from $0 - 10000$m in the inline direction.

Figures 10 displays the magnitude and phase of the inline electric field. The effect of the resistor is clearly present in the signal compared to the correct anisotropic background. Figure 11 shows the normalized amplitude and phase difference with respect to the true background and three isotropic background models with the same structure. The three isotropic models are chosen with the horizontal conductivity, the vertical conductivity and a conductivity in between ($\sigma = 1$S/m) in the anisotropic layer, respectively. This is done to study the differences in the the normalized fields and phase differences with respect to the isotropic models compared to the true anisotropic model.

From Figures 11(a) and 11(b) we observe that the curves with respect to the isotropic models follow a pattern with decreasing conductivity in the overburden. However, the curve corresponding to the anisotropic background does not seem to follow this pattern, indicating that the TIV anisotropy introduces an effect that is difficult to explain with isotropic models with the same structure. This is in compliance with Ramananjaona et al. (2010), and may lead to wrong interpretations if the anisotropy is not properly accounted for. Assuming that an anomaly is discovered if the normalized mangnitude exceeds 1.3, which is the same threshold as used in Roth and Maaø (2007), we see that when using the anisotropic background the anomaly is discovered. The following negative anomaly is due to the airwave (Roth and Maaø, 2007). The models using $\sigma = \sigma_h$ and $\sigma = 1$S/m yields a higher peak for the normalized response, but in a completely different position. This may lead to wrongful conclusions when interpreting the signal. The model using $\sigma = \sigma_v$ however, does not

pass the 1.3 limit. A reservoir may thus be screened by anisotropy in the overburden if it is not accounted for.

DISCUSSION

The examples demonstrate that TIV anisotropy has a significant effect on mCSEM data. It should thus be taken into account when modeling such experiments to possibly avoid wrongful interpretations, for example anomaly screening due to anisotropic formations in the overburden. This method constitutes a possible method for taking into account TIV anisotropy in the 2.5D setting, and may also be extended to more general anisotropy configurations.

However, this method's computational advantage decreases rapidly as the complexity of the background increases, as it relies on rapid construction of the Green's tensors and evaluation of the integrals. Thus, with complex background models the method might not be as efficient compared to other approaches using finite differences or finite elements. Moreover, the 2.5D approach is, of course, not sufficient in complex areas where the true 3D nature of the experiment is significant. The method will not produce results that are comparable to scattering experiments with significant 3D scattering effects due to cross line variations.

CONCLUSIONS

We have demonstrated a 2.5D integral equation modeling framework for frequency domain electromagnetic field propagation in TIV conductive media with conductivity contrasts. We find that the framework is capable of simulating mCSEM experiments for hydrocarbon prospecting in TIV models with respect to model size and conductivity ranges, and that one only has to solve between 20 and 30 2D problems to obtain reasonable results. This should prove computationally efficient compared to solving the full 3D problem and is in compliance with earlier work on 2.5D modeling.

The numerical experiments demonstrate that TIV anisotropy has a significant effect on mCSEM data, while the added computational complexity in modeling is minimal. Thus, TIV anisotropy should be taken into account in mCSEM modeling, and it may be necessary to avoid wrongful conclusions. For instance, the final numerical example shows that anomalies may be screened by the presence of TIV anisotropy in the overburden. The presented method constitutes an option for taking TIV anisotropy into account when modeling mCSEM data under the given assumptions, and could be useful both for survey planning, interpretation and inversion.

ACKNOWLEDGEMENTS

Torgeir Wiik wishes to thank Lars Ole Løseth (Statoil ASA) for valuable discussions concerning modeling and anisotropy. He also acknowledges Statoil ASA for sponsoring his Ph.D. project. Bjørn Ursin has received financial support from the VISTA project

and from the Norwegian Research Council through the ROSE project.

REFERENCES

Abubakar, A., T. M. Habashy, V. L. Druskin, L. Knizhnerman, and D. Alumbaugh, 2008, 2.5D forward and inverse modeling for interpreting low-frequency electromagnetic measurements: Geophysics, **73**, F165–F177.

Abubakar, A., and P. M. van den Berg, 2004, Iterative forward and inverse algorithms based on domain integral equations for three-dimensional electric and magnetic objects: Journal of Computational Physics, **195**, 236–262.

Abubakar, A., P. M. van den Berg, and T. M. Habashy, 2006, An integral equation approach for 2.5-dimensional forward and inverse electromagnetic scattering: Geophysical Journal International, **165**, 744–762.

Colton, D., and R. Kress, 1992, Inverse acoustic and electromagnetic inverse scattering theory: Springer Verlag.

Eidesmo, T., S. Ellingsrud, L. M. MacGregor, S. Constable, M. C. Sinha, S. Johansen, F. N. Kong, and H. Westerdal, 2002, Sea Bed Logging (SBL), a new method for remote and direct idetification of hydrocarbon filled layers in deepwater areas: First Break, **20**, 144–152.

Green, G., 1828, An essay on the application of mathematical analysis to the theories of electricity and magnetism: T. Wheelhouse, Nottingham.

Hohmann, G. W., 1971, Electromagnetic scattering by conductors in the earth near a line source of current: Geophysics, **36**, 101–131.

———, 1975, Three-dimensional induced polarization and electromagnetic modeling: Geophysics, **40**, 309–324.

———, 1983, Three-dimensional EM Modeling: Geophysical Surveys, **6**, 27–53.

———, 1987, Numerical modeling for electromagnetic methods of geophysics, *in* Electromagnetic Methods in Applied Geophysics. Volume 1, Theory: SEG, 313–363.

Kong, F. N., S. E. Johnstad, T. Røsten, and H. Westerdal, 2008, A 2.5D finite-element-modeling difference method for marine csem modeling in stratified anisotropic media: Geophysics, **73**, F9–F19.

Kong, F. N., H. Westerdal, S. Ellingsrud, T. Eidesmo, and S. E. Johansen, 2002, Seabed logging: a possible direct hydrocarbon indicator for deepsea prospects using EM energy: Oil & Gas Journal of Computational Physics, **100**, 30–38.

Li, Y., and K. Key, 2007, 2d marine controlled-source electromagnetic modeling: Part 1 an adaptive finite-element algorithm: Geophysics, **72**, WA51–WA62.

Løseth, L. O., 2007, Modelling of controlled source electromagnetic data: PhD thesis, Norwegian University of Science and technology.

Løseth, L. O., and B. Ursin, 2007, Electromagnetic fields in planarly layered anisotropic media: Geophysical Journal International, **170**, 44–80.

Mitsuhata, Y., 2000, 2-D electromagnetic modeling by finite-element method with a dipole source and topography: Geophysics, **65**, 465–475.

Nabighian, M. N., ed., 1987, Electromagnetic methods in applied geophysics: SEG.

Negi, J. G., and P. D. Saraf, 1989, Anisotropy in geoelectromagnetism: Elsevier, New York.

Ramananjaona, C., L. MacGregor, and D. Andreis, 2010, Sensitivity and inversion of marine electromagnetic data in a vertically anisotropic stratified earth: Geophysical Prospecting, **Published online**, DOI: 10.1111/j.1365–2478.2010.00919.x.

Roth, F., and F. Maaø, 2007, Improving seabed logging sensitivity in shallow water through up-down separation: EGM 2007 International Workshop, **1**.

Stoyer, C. H., and R. J. Greenfield, 1976, Numerical solutions of the response of a two-dimensional earth to an oscillating magnetic dipole source: Geophysics, **41**, 519–530.

Stratton, J. A., 1941, Electromagnetic theory: McGraw-Hill.

Tehrani, A. M., and E. Slob, 2008, Modeling in-line data for seabed logging with 2.5d and 3d integral equations: SEG Expanded Abstracts, **27**, doi:10.1190/1.3063746.

Unsworth, M. J., B. J. Travis, and A. D. Chave, 1993, Electromagnetic induction by a finite electric dipole source over a 2-d earth: Geophysics, **58**, 198–214.

Ursin, B., 1983, Review of elastic and electromagnetic wave propagation in horizontally layered media: Geophysics, **48**, 1063–1081.

van den Berg, P. M., 1984, Iterative computational techniques in scattering based upon the integrated square error criterion: IEEE Transactions on Antennas and Propagation, **32**, 1063–1071.

Zhdanov, M. S., 2002, Geophysical inverse theory and regularization problems: Elsevier.

Figure 1: Schematic intersection of the model.

Figure 2: Model used in benchmark of 2.5D code against 1D code.

Figure 3: Inline electric field from benchmark of 2.5D code against 1D code. 2.5D with anisotropy (red cross), 1D with anisotropy (blue circle) and isotropic 1D with $\sigma = \sigma_h$ (black triangle). (a) Amplitude, (b) Phase.

Figure 4: 2.5D inline electric field compared to true 1D model in benchmark example. (a) Normalized amplitude, (b) Phase difference.

Figure 5: Vertical electric field from benchmark of 2.5D code against 1D code. 2.5D with anisotropy (red cross), 1D with anisotropy (blue circle) and isotropic 1D with $\sigma = \sigma_h$ (black triangle). (a) Amplitude, (b) Phase.

Figure 6: 2.5D vertical electric field compared to true 1D model in benchmark example. (a) Normalized amplitude, (b) Phase difference.

Figure 7: 2.5D inline electric field from the model from Figure 8 in Kong et al. (2008) compared to 1D model without target. 2.5D results (red cross) and 1D results (blue circle). (a) Amplitude, (b) Phase.

Figure 8: 2.5D inline electric field from the model from Figure 8 in Kong et al. (2008) compared to 1D model with target. 2.5D results (red cross) and 1D results (blue circle). (a) Amplitude, (b) Phase.

Figure 9: Model used for test of anisotropy in overburden above resistor.

Figure 10: Inline electric field from test of anisotropy in overburden. Model with resistor (blue circle), model without resistor (red cross). (a) Amplitude, (b) Phase.

Figure 11: Inline electric field from test of anisotropy in overburden compared to different models without reservoir. Response compared to true TIV background

(blue circles), against isotropic model with horizontal conductivity (red cross), against isotropic model with vertical conductivity (green stars), against isotropic model with conductivity between σ_h and σ_v in the anisotropic layer (black triangle). (a) Normalized amplitude, (b) Phase difference.

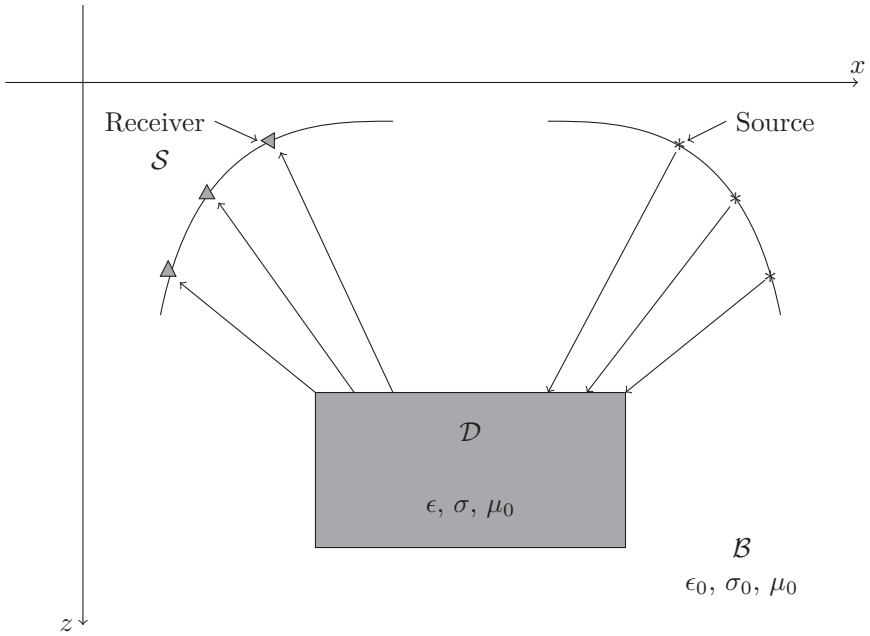

Figure 1: Schematic intersection of the model.

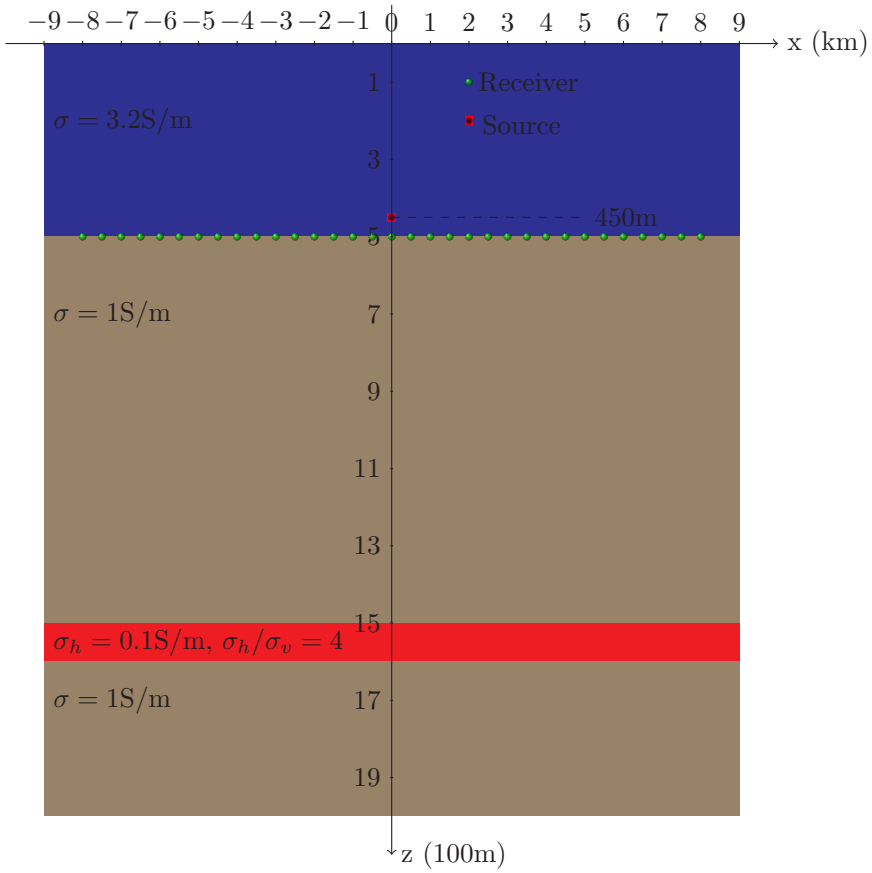

Figure 2: Model used in benchmark of 2.5D code against 1D code.

(a)

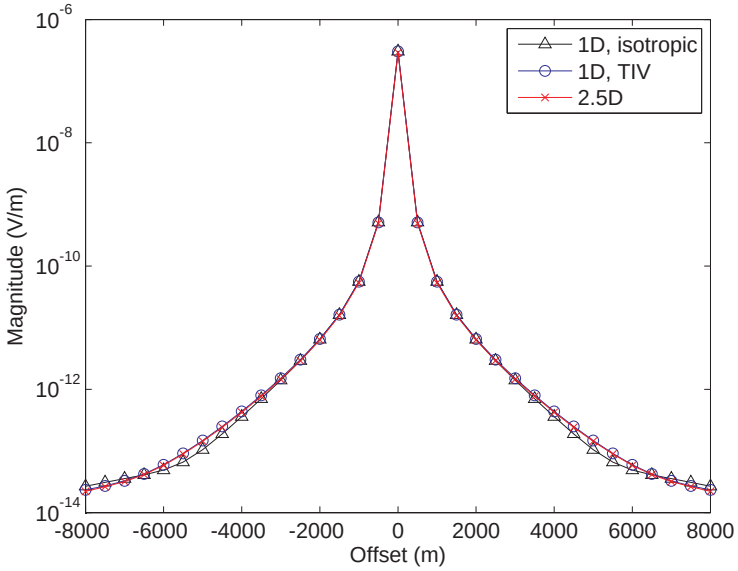

(b)

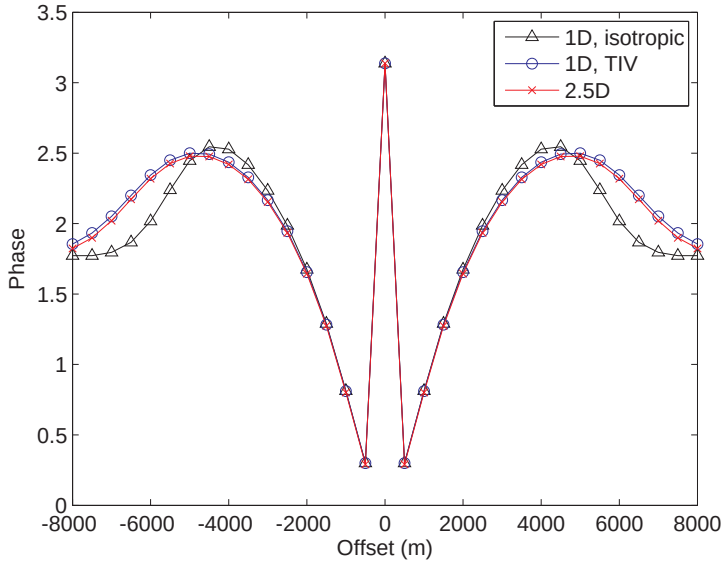

Figure 3: Inline electric field from benchmark of 2.5D code against 1D code. 2.5D with anisotropy (red cross), 1D with anisotropy (blue circle) and isotropic 1D with $\sigma = \sigma_h$ (black triangle). (a) Amplitude, (b) Phase.

(a)

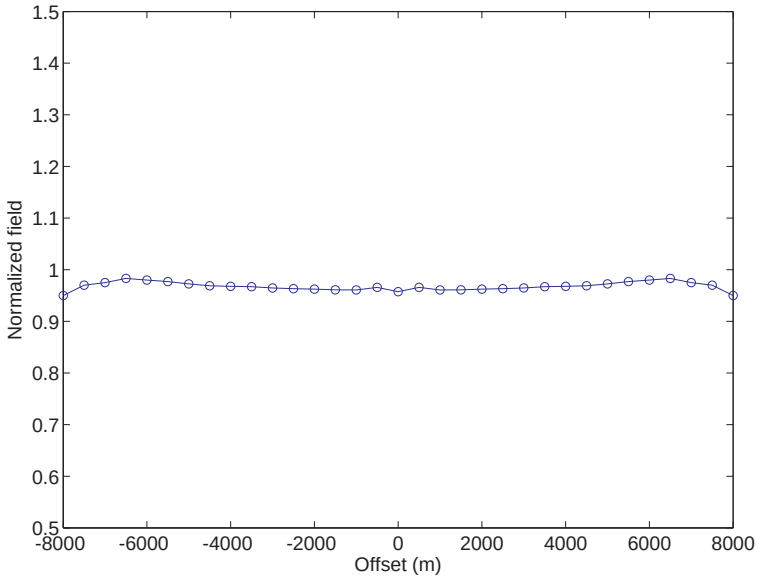

(b)

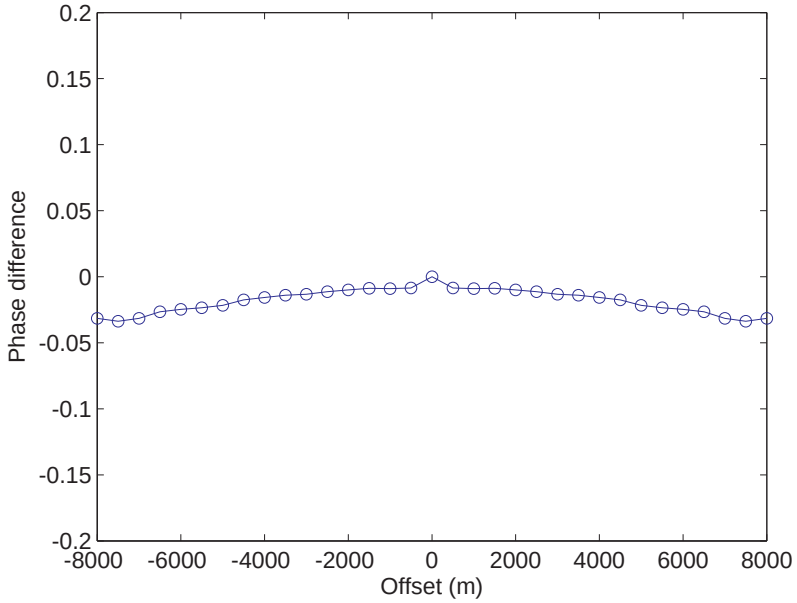

Figure 4: 2.5D inline electric field compared to true 1D model in benchmark example.

(a) Normalized amplitude, (b) Phase difference.

(a)

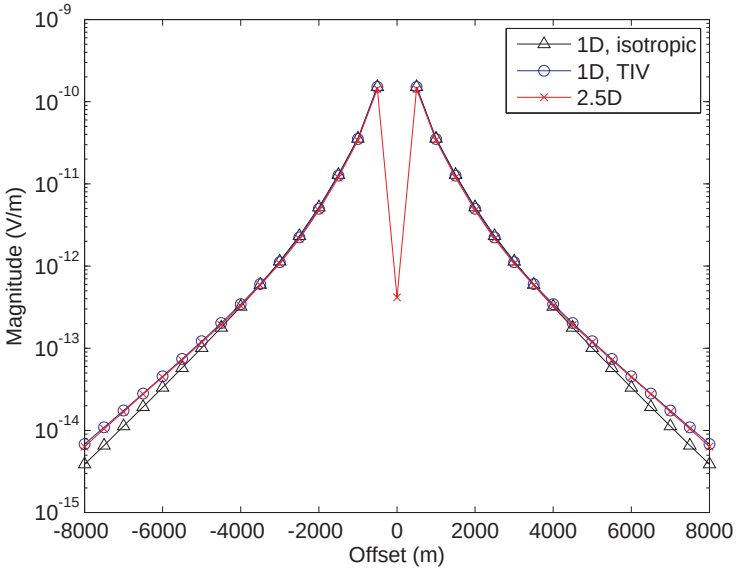

(b)

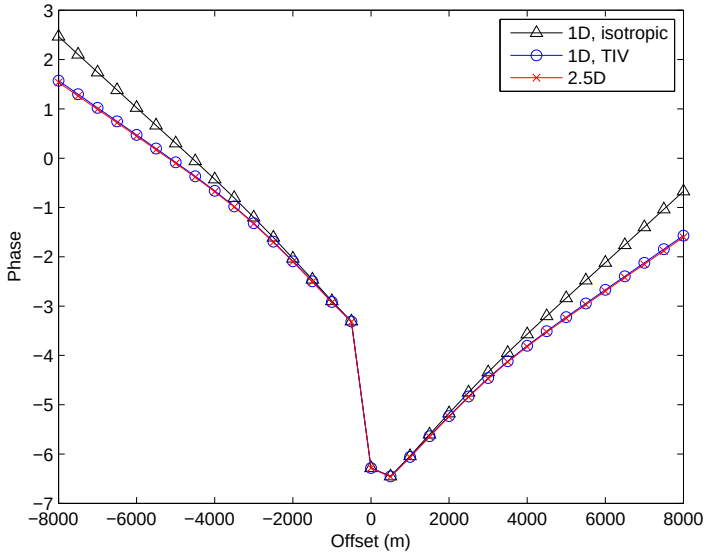

Figure 5: Vertical electric field from benchmark of 2.5D code against 1D code. 2.5D with anisotropy (red cross), 1D with anisotropy (blue circle) and isotropic 1D with $\sigma = \sigma_h$ (black triangle). (a) Amplitude, (b) Phase.

(a)

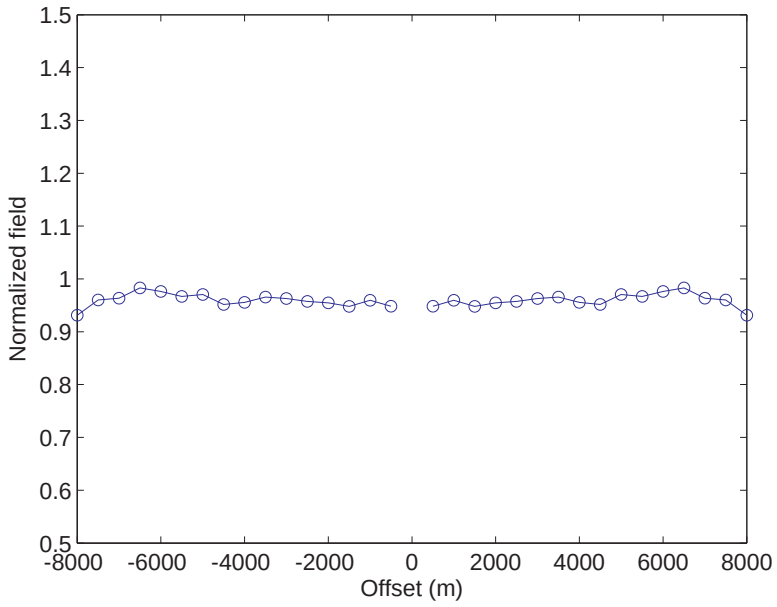

(b)

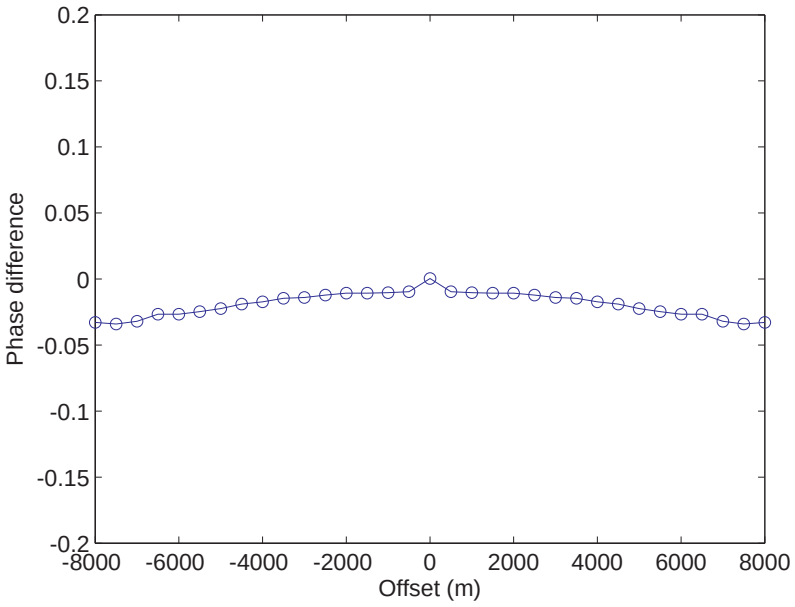

Figure 6: 2.5D vertical electric field compared to true 1D model in benchmark example. (a) Normalized amplitude, (b) Phase difference.

(a)

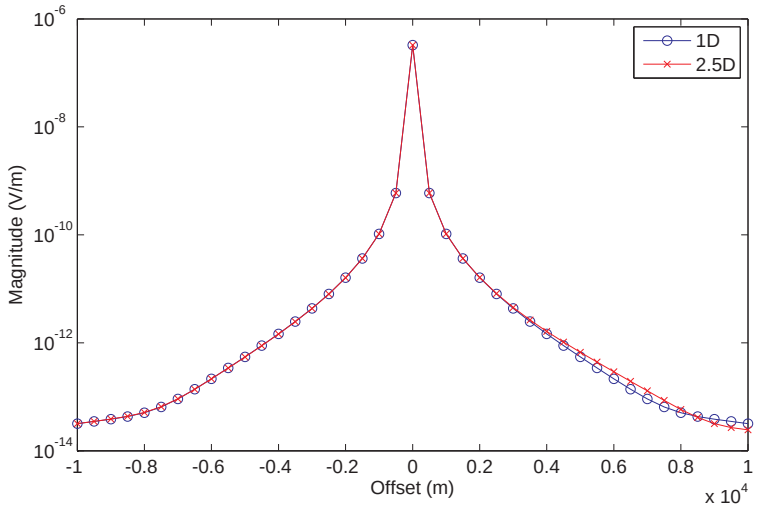

(b)

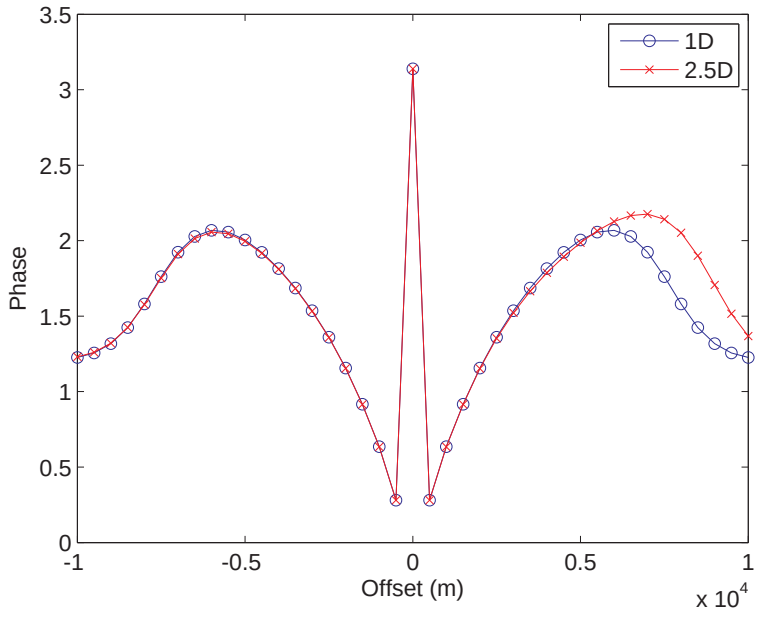

Figure 7: 2.5D inline electric field from the model from Figure 8 in Kong et al. (2008) compared to 1D model without target. 2.5D results (red cross) and 1D results (blue circle). (a) Amplitude, (b) Phase.

(a)

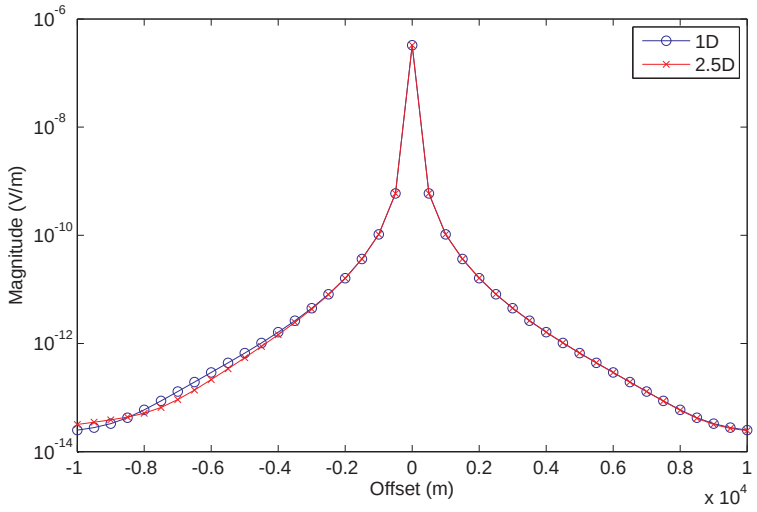

(b)

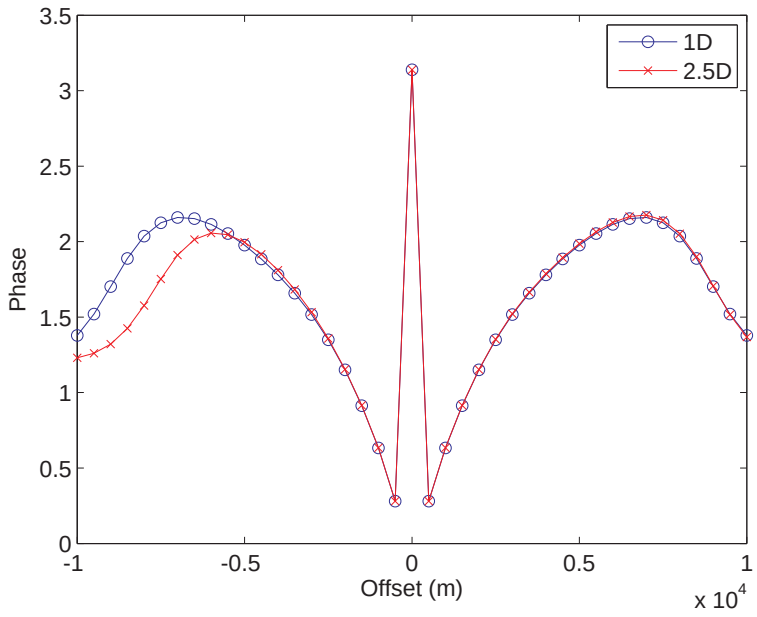

Figure 8: 2.5D inline electric field from the model from Figure 8 in Kong et al. (2008) compared to 1D model with target. 2.5D results (red cross) and 1D results (blue circle). (a) Amplitude, (b) Phase.

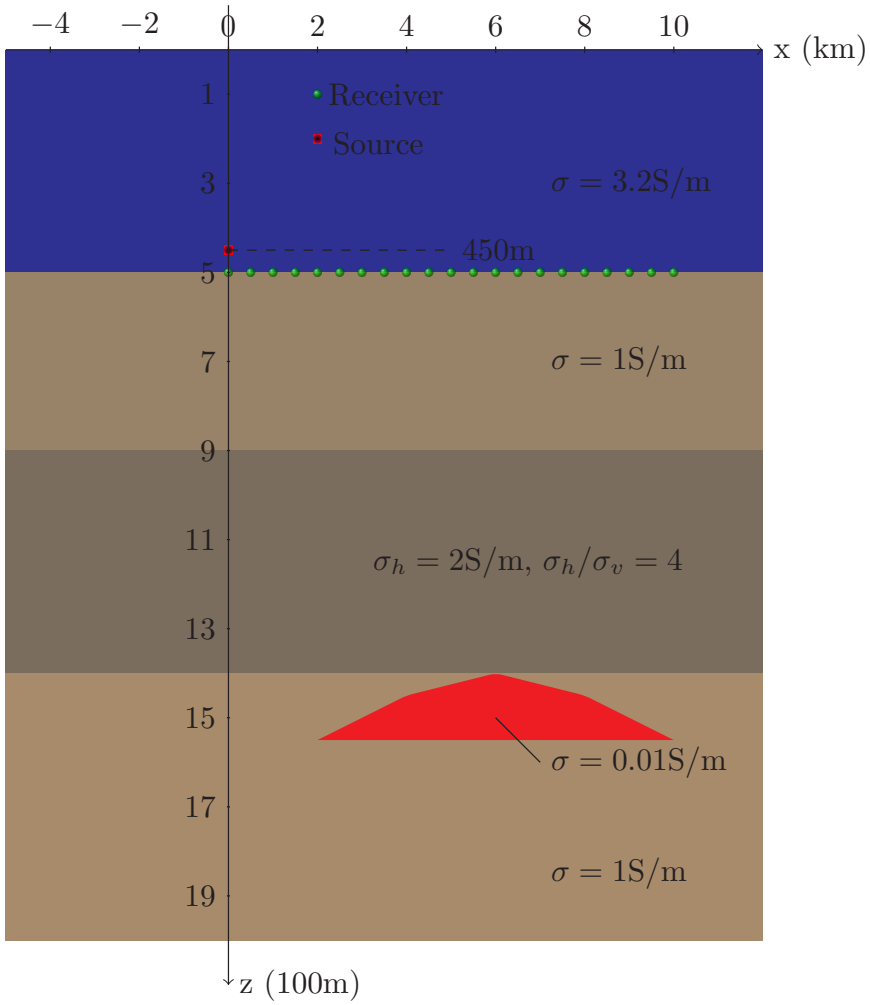

Figure 9: Model used for test of anisotropy in overburden above resistor.

(a)

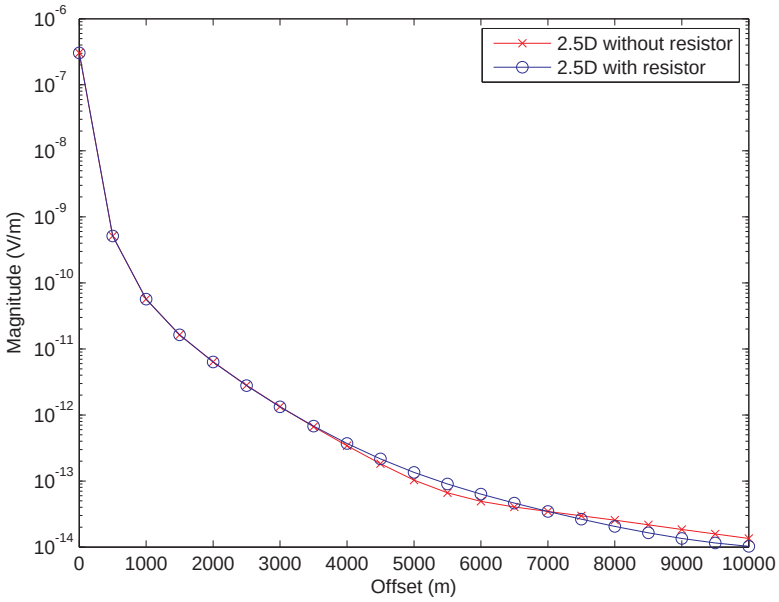

(b)

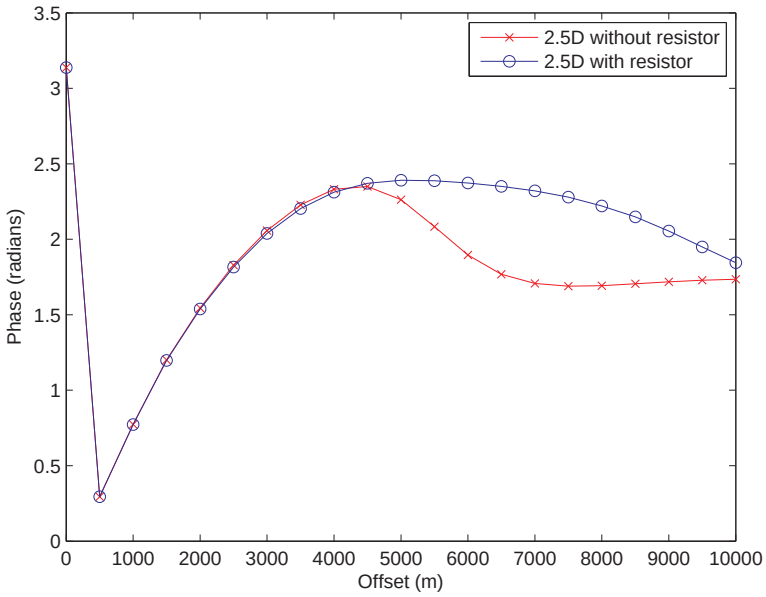

Figure 10: Inline electric field from test of anisotropy in overburden. Model with resistor (blue circle), model without resistor (red cross). (a) Amplitude, (b) Phase.

(a)

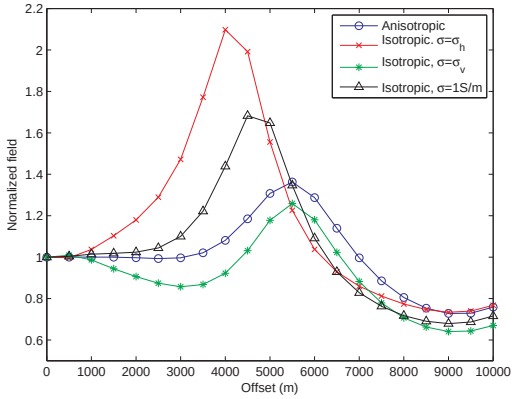

(b)

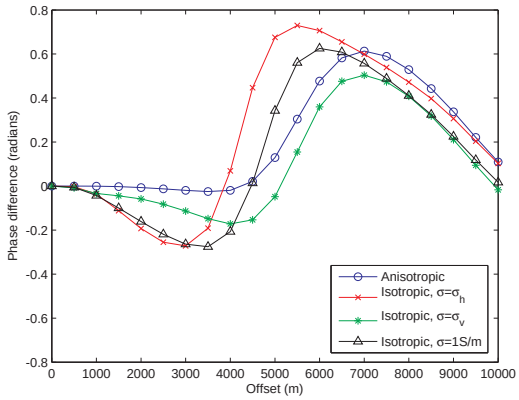

Figure 11: Inline electric field from test of anisotropy in overburden compared to different models without reservoir. Response compared to true TIV background (blue circles), against isotropic model with horizontal conductivity (red cross), against isotropic model with vertical conductivity (green stars), against isotropic model with conductivity between σ_h and σ_v in the anisotropic layer (black triangle). (a) Normalized amplitude, (b) Phase difference.